Supporting Information for

Prediction and characterization of $NaGaS_2$, a high thermal conductivity mid-infrared nonlinear optical material for high-power laser frequency conversion

Dianwei Hou,[†] Arun S Nissimagoudar,[‡] Qiang Bian,[†] Kui Wu,[†] Shilie Pan,[*,†] Wu Li,[*,‡] and Zhihua Yang[*,†]

†CAS Key Laboratory of Functional Materials and Devices for Special Environments, Xinjiang Technical Institute of Physics & Chemistry, CAS; Xinjiang Key Laboratory of Electronic Information Materials and Devices, 40-1 South Beijing Road, Urumqi 830011, China.

‡Institute for Advanced Study, Shenzhen University, Shenzhen 518060, People's Republic of China

1. Computational details

a) Structure Search

The search for the global minimum structure carried out at ambient pressure for Na-Ga-S ternary system with molar ratio 1:1:2 and cell sizes 1-6, implemented in CALYPSO package[1-2]. In a typical CALYPSO calculation, each generation contained 30 structures, in which 60% of the lower enthalpy structures were utilized to create the structures in the next generation by artificial bee colony algorithm, with the rest 40% structures generated randomly. A population of structures belonging to certain space group symmetries in the first generation are produced randomly. The structure search for each cell size was stopped after 30 generations iteratively. All the structures generated by CALYPSO are locally optimized using the Vienna Ab initio Simulation Package (VASP) code[3], with an economy set of input parameters and an energy convergence threshold of 1×10^{-5} eV per cell.

b) Structural optimization and phonon spectrum

Thirty structures with lower enthalpies in each cell size are selected and further optimized with high accuracy using density functional theory within the generalized gradient approximation as implemented in the VASP code. The plane wave cutoff energy is set as 800 eV in the calculation, and the Monkhorst-Pack *k*-mesh with a maximum spacing of 0.16 $Å^{-1}$ was individually adjusted in reciprocal space in respect of the size of each computational cell. The phonon dispersion curve was calculated through finite displacement approach as implemented in the Phonopy code[4-5]. The absence of imaginary frequency in the whole Brillouin zone indicated the dynamic stability of the title compound.

c) Electronic band structures and optical properties

Electronic, linear optical and nonlinear optical properties were calculated with the CASTEP package[6] for the global minimum structure, $NaGaS_2$. As band gap has a significant influence on optical properties, the screened exchange local density approximation (i.e., sX-LDA)[7] method is employed to calculate band gap of the semiconductors. Furthermore, the SHG coefficients are calculated using an expression

originally proposed by Rashkeev et al. and developed by Zhang et al.[8] The second order susceptibility $\chi_{ijk}^{(2)}$ is represented as:

$$\chi_{ijk}^{(2)} = \chi_{ijk}^{(2)}(VE) + \chi_{ijk}^{(2)}(VH)$$

where $\chi_{ijk}^{(2)}(VE)$ and $\chi_{ijk}^{(2)}(VH)$ indicate the contributions from virtual electron processes and virtual hole processes, respectively. Formulas for calculating $\chi_{ijk}^{(2)}(VE)$ and $\chi_{ijk}^{(2)}(VH)$ are as following:

$$\chi_{ijk}^{(2)}(\mathrm{VE}) = \frac{e^3}{2\hbar m^3} \sum_{vcc'} \int \frac{d^3k}{4\pi^3} P(ijk)\, \mathrm{Im}\left[P_{cv}^{i} P_{cc'}^{j} P_{c'v}^{k} \right] \left(\frac{1}{\omega_{cv}^{3} \omega_{vc'}^{2}} + \frac{2}{\omega_{vc}^{4} \omega_{c'v}} \right)$$

$$\chi_{ijk}^{(2)}(\mathrm{VH}) = \frac{e^3}{2\hbar m^3} \sum_{vv'c} \int \frac{d^3k}{4\pi^3} P(ijk)\, \mathrm{Im}\left[P_{vv'}^{i} P_{cv'}^{j} P_{cv}^{k} \right] \left(\frac{1}{\omega_{cv}^{3} \omega_{v'c}^{2}} + \frac{2}{\omega_{vc}^{4} \omega_{cv'}} \right)$$

Here, *i*, *j*, *k* are Cartesian components, v and v' indicate valence band, and *c* and *c*' denote conduct band. *P*(*ijk*) denotes full permutation. The band energy difference and momentum matrix elements between the electronic states α and β are demonstrated as $\hbar\omega_{\alpha\beta}$ and $P_{\alpha\beta}^{n}$, respectively, and they are implicitly *k*-point dependent. It should be emphasized that the refractive indices and second harmonic generation coefficients can be accurately obtained by density functional theory in principle because these optical properties are determined by the virtual electronic excited processes which are described by the first and second order perturbations, respectively, on the ground state wave functions.[9]

Table S1. Structure parameters of $NaGaS_2$ and $Na_4Ga_4S_8$

Compounds	Space group	Lattice Parameters (Å)	Atom	Site	Atomic positions
$NaGaS_2$	I-42D	a=b=6.350 c=9.548	Na	4b	0.50000 1.00000 0.25000
			Ga	4a	1.00000 0.50000 0.25000
			S	8d	0.75000 0.81116 0.87500
$Na_4Ga_4S_8$	P41212	a=b=6.415 c=9.308	S	8b	0.23126 0.83205 0.53188
			Na	4a	0.29157 0.70843 0.25000
			Ga	4a	0.81112 0.81112 0.00000

Note: The energy of compound $Na_4Ga_4S_8$ has a higher value of 0.026 eV/atom than that of $NaGaS_2$

Table S2. The formation enthalpies of reaction pathway for $NaGaS_2$

Reaction pathway	Formation enthalpy (eV/atom)
$NaS + GaS = NaGaS_2$	-0.214
$NaGa_4 + NaS + 5\ Ga_2S_3 = 14\ NaGaS_2$	-0.377
$Na_2S + Ga_2S_3 = 2\ NaGaS_2$	-0.093
$Na_2S_2 + 2\ GaS = 2\ NaGaS_2$	-0.214
$2\ NaGa_4 + 13\ Na_2S_2 + 10\ Ga_2S_3 = 28\ NaGaS_2$	-0.377
$2\ NaGa_4 + 5\ Na_2S_4 + 4\ GaS = 12\ NaGaS_2$	-0.720
$13\ Na_2S_4 + 4\ Ga_2S_3 = 32\ NaGaS_2$	-1.102
$3\ NaGa_4 + 5\ Na_2S_5 + GaS = 13\ NaGaS_2$	-1.570
$8\ NaGa_4 + 13\ Na_2S_5 + Ga_2S_3 = 34\ NaGaS_2$	-1.575
$Na_{22}Ga_{39} + 139\ NaS + 61\ Ga_2S_3 = 161\ NaGaS_2$	-0.324
$Na_2S + Ga_2S_3 = 2\ NaGaS_2$	-0.093
$Na_2S_2 + 2\ GaS = 2\ NaGaS_2$	-0.214
$2\ Na_{22}Ga_{39} + 139\ Na_2S_2 + 122\ Ga_2S_3 = 322\ NaGaS_2$	-0.323
$2\ Na_{22}Ga_{39} + 61\ Na_2S_4 + 88\ GaS = 166\ NaGaS_2$	-0.536
$6\ Na_{22}Ga_{39} + 139\ Na_2S_4 + 88\ Ga_2S_3 = 410\ NaGaS_2$	-0.573
$3\ Na_{22}Ga_{39} + 61\ Na_2S_5 + 71\ GaS = 188\ NaGaS_2$	-1.194
$8\ Na_{22}Ga_{39} + 139\ Na_2S_5 + 71\ Ga_2S_3 = 454\ NaGaS_2$	-1.184
$Na_7Ga_{13} + 46\ NaS + 20\ Ga_2S_3 = 53\ NaGaS_2$	-0.329
$Na_7Ga_{13} + 23\ Na_2S_2 + 20\ Ga_2S_3 = 53\ NaGaS_2$	-0.325
$Na_7Ga_{13} + 10\ Na_2S_4 + 14\ GaS = 27\ NaGaS_2$	-0.543
$3\ Na_7Ga_{13} + 23\ Na_2S_4 + 14\ Ga_2S_3 = 67\ NaGaS_2$	-0.580
$3\ Na_7Ga_{13} + 20\ Na_2S_5 + 22\ GaS = 61\ NaGaS_2$	-1.210
$4\ Na_7Ga_{13} + 23\ Na_2S_5 + 11\ Ga_2S_3 = 74\ NaGaS_2$	-1.202

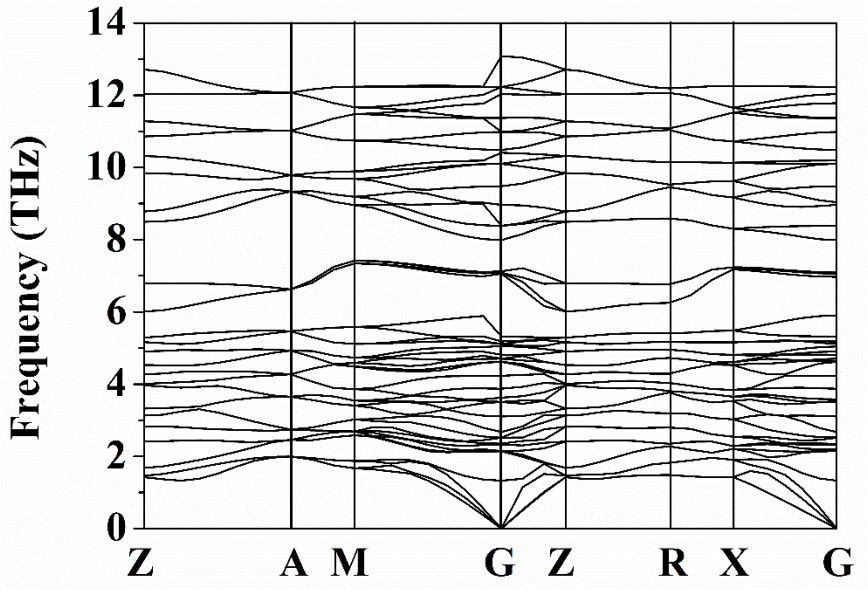

Figure S1. Calculated phonon dispersion curves of compound $Na_4Ga_4S_8$

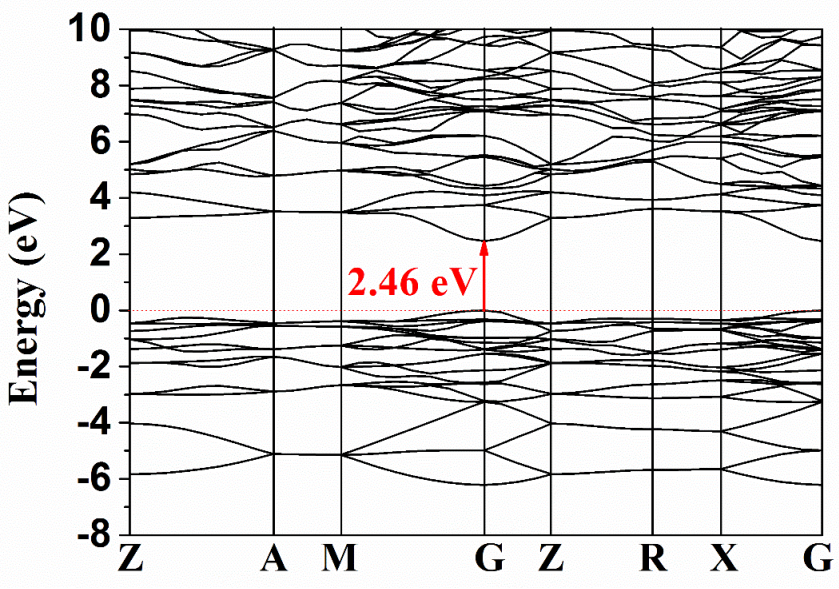

Figure S2. Calculated electronic band structure of compound $NaGaS_2$

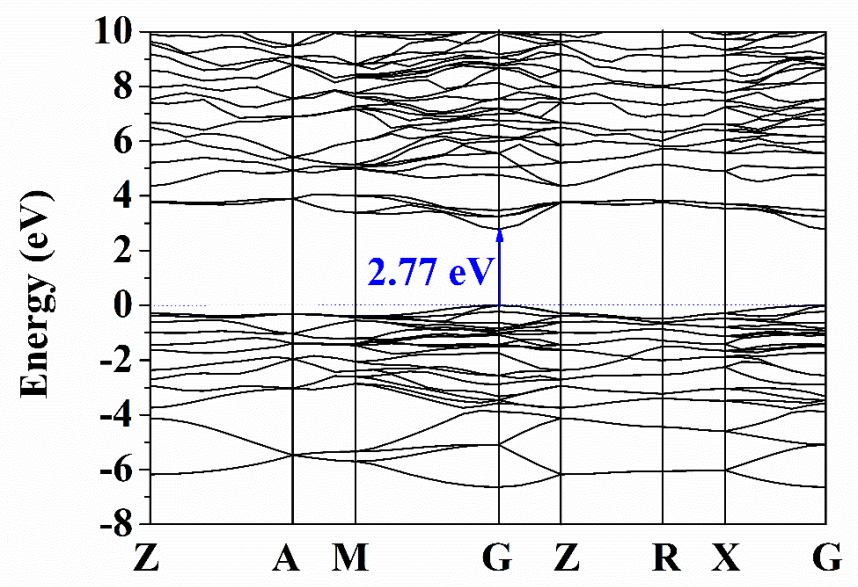

Figure S3. Calculated electronic band structure of compound $Na_4Ga_4S_8$

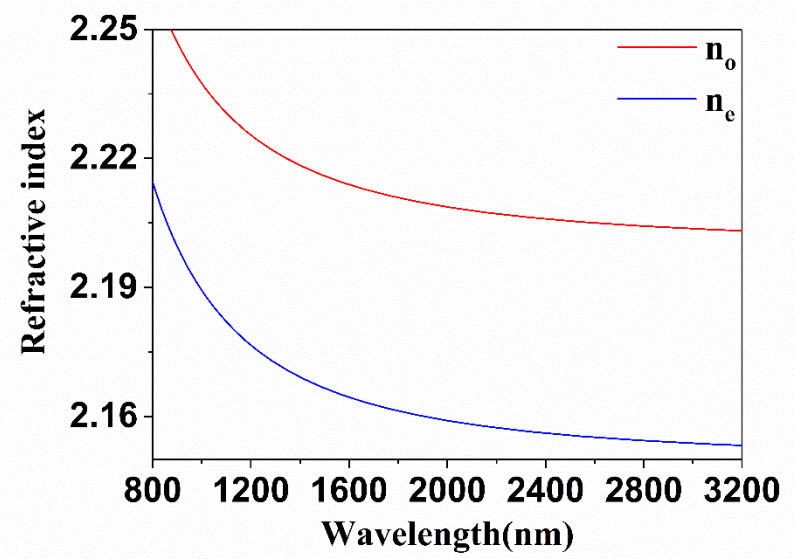

Figure S4. Calculated refractive index of compound $NaGaS_2$

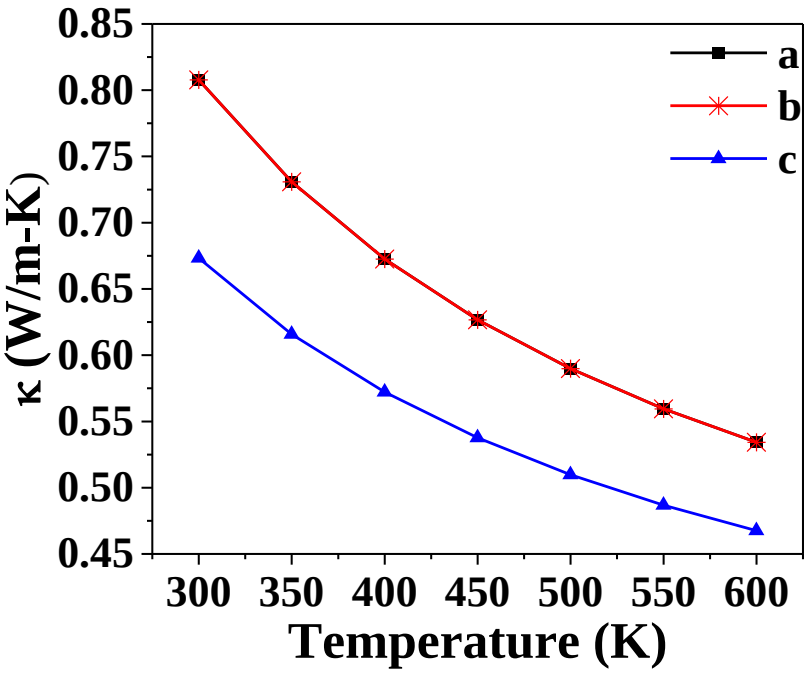

Figure S5 (a). Thermal conductivity of IR NLO crystal $AgGaS_2$ calculated with ShengBTE code. Direction of *a* and *b* have the same thermal conductivity values and these two lines are overlapping

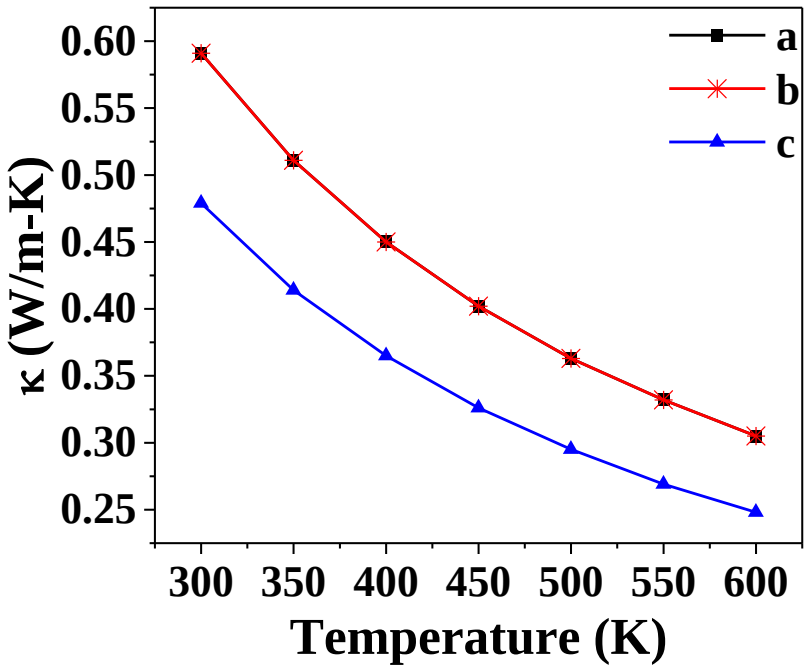

Figure S5 (b). Thermal conductivity of IR NLO crystal $AgGaSe_2$ calculated with ShengBTE code. Direction of *a* and *b* have the same thermal conductivity values and these two lines are overlapping

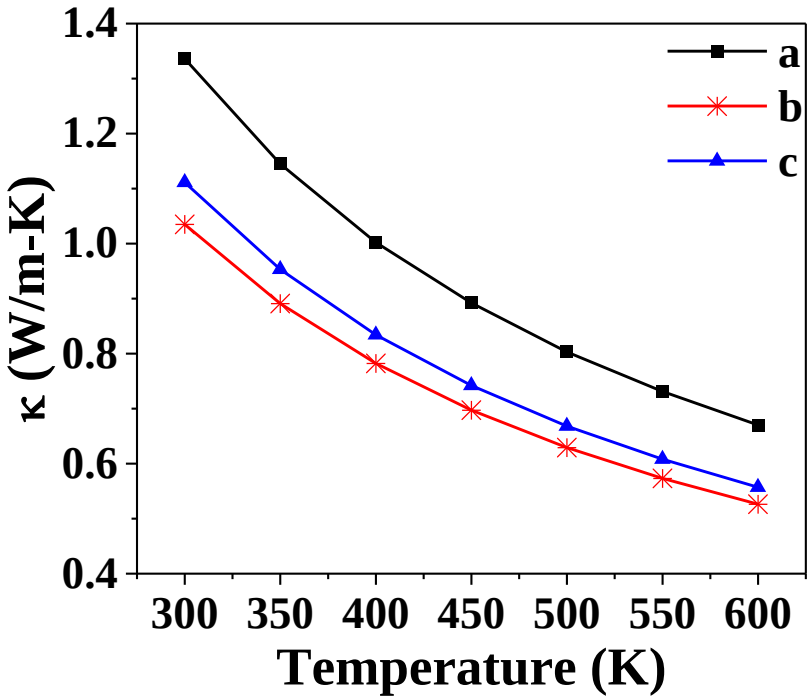

Figure S5 (c). Thermal conductivity of IR NLO crystal $LiGaS_2$ calculated with ShengBTE code

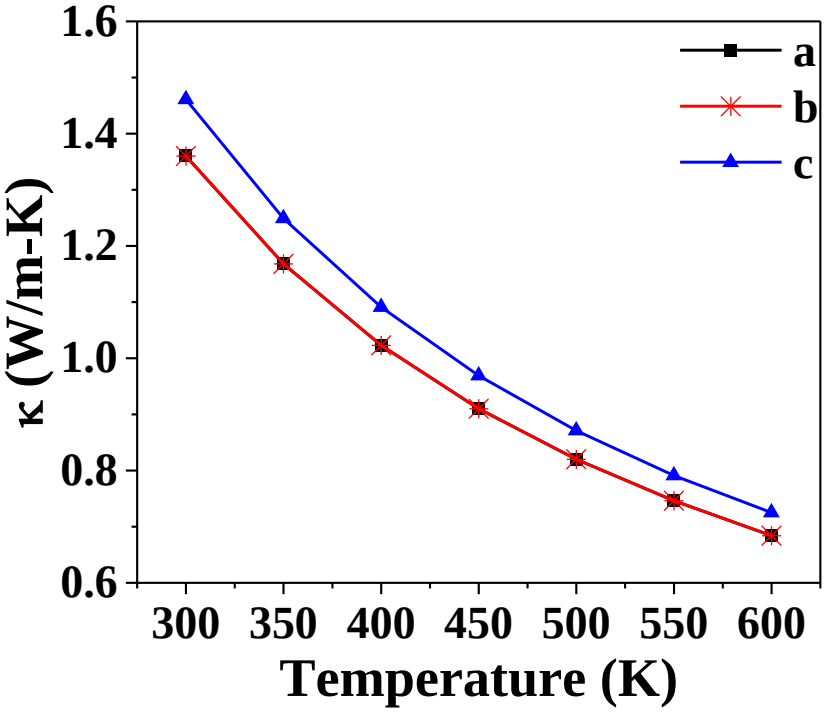

Figure S5 (d). Thermal conductivity of IR NLO crystal $NaGaS_2$ calculated with ShengBTE code. Direction of *a* and *b* have the same thermal conductivity values and these two lines are overlapping

References

(1) Wang, Y.; Lv, J.; Zhu, L.; Ma, Y., Crystal structure prediction via particle-swarm optimization. *Phys. Rev. B* **2010,** *82*, 094116.

(2) Wang, Y.; Lv, J.; Zhu, L.; Ma, Y., CALYPSO: A method for crystal structure prediction. *Comput. Phys. Commun.* **2012,** *183*, 2063-2070.

(3) Kresse, G.; Furthmüller, J., Efficient iterative schemes for ab initio total-energy calculations using a plane-wave basis set. *Phys. Rev. B* **1996,** *54*, 11169-11186.

(4) Togo, A.; Tanaka, I., First principles phonon calculations in materials science. *Scripta Mater.* **2015,** *108*, 1-5.

(5) Togo, A.; Oba, F.; Tanaka, I., First-principles calculations of the ferroelastic transition between rutile-type and $CaCl_2$-type SiO_2 at high pressures. *Phys. Rev. B* **2008,** *78*, 134106.

(6) Segall, M. D.; Philip, J. D. L.; Probert, M. J.; Pickard, C. J.; Hasnip, P. J.; Clark, S. J.; Payne, M. C., First-principles simulation: ideas, illustrations and the CASTEP code. *J. Phys.: Condens. Matter* **2002,** *14*, 2717.

(7) Asahi, R.; Mannstadt, W.; Freeman, A. J., Optical properties and electronic structures of semiconductors with screened-exchange LDA. *Phys. Rev. B* **1999,** *59*, 7486-7492.

(8) Zhang, B.; Lee, M.-H.; Yang, Z.; Jing, Q.; Pan, S., Simulated pressure-induced blue-shift of phase-matching region and nonlinear optical mechanism for $K_3B_6O_{10}X$ (X= Cl, Br). *Appl. Phys. Lett.* **2015,** *106*, 031906.

(9) Kang, L.; Zhou, M.; Yao, J.; Lin, Z.; Wu, Y.; Chen, C., Metal thiophosphates with good mid-infrared nonlinear optical performances: A first-principles prediction and analysis. *J. Am. Chem. Soc.* **2015,** *137* (40), 13049-13059.